A&A 600, A15 (2017)
DOI: 10.1051/0004-6361/201629066
© ESO 2017

Astronomy & Astrophysics

HC_3N observations of nearby galaxies

Xue-Jian Jiang (蒋雪健)[1,5], Jun-Zhi Wang (王均智)[2], Yu Gao (高煜)[1,5], and Qiu-Sheng Gu (顾秋生)[3,4,5]

[1] Purple Mountain Observatory & Key Laboratory for Radio Astronomy, Chinese Academy of Sciences, 2 West Beijing Road, 210008 Nanjing, PR China
e-mail: xjjiang@pmo.ac.cn
[2] Shanghai Astronomical Observatory, Chinese Academy of Sciences, 80 Nandan Road, 200030 Shanghai, PR China
[3] School of Astronomy and Space Sciences, Nanjing University, 210093 Nanjing, PR China
[4] Key Laboratory of Modern Astronomy and Astrophysics (Nanjing University), Ministry of Education, 210093 Nanjing, PR China
[5] Collaborative Innovation Center of Modern Astronomy and Space Exploration, 210093 Nanjing, PR China

Received 7 June 2016 / Accepted 22 December 2016

ABSTRACT

Aims. We aim to systematically study the properties of the different transitions of the dense molecular gas tracer HC_3N in galaxies.
Methods. We have conducted single-dish observations of HC_3N emission lines towards a sample of nearby gas-rich galaxies. $HC_3N(J = 2-1)$ was observed in 20 galaxies with the Effelsberg 100-m telescope. $HC_3N(J = 24-23)$ was observed in nine galaxies with the 10-m Submillimeter Telescope (SMT).
Results. HC_3N 2−1 is detected in three galaxies: IC 342, M 66, and NGC 660 ($>3\sigma$). HC_3N 24−23 is detected in three galaxies: IC 342, NGC 1068, and IC 694. These are the first measurements of HC_3N 2−1 in a relatively large sample of external galaxies, although the detection rate is low. For the HC_3N 2−1 non-detections, upper limits (2σ) are derived for each galaxy, and stacking the non-detections is attempted to recover the weak signal of HC_3N. The stacked spectrum, however, does not show any significant signs of HC_3N 2−1 emission. The results are also compared with other transitions of HC_3N observed in galaxies.
Conclusions. The low detection rate of both transitions suggests low abundance of HC_3N in galaxies, which is consistent with other observational studies. The comparison between HC_3N and HCN or HCO^+shows a large diversity in the ratios between HC_3N and HCN or HCO^+. More observations are needed to interpret the behavior of HC_3N in different types of galaxies.

Key words. galaxies: active – galaxies: ISM – galaxies: evolution – ISM: molecules

1. Introduction

Molecular lines play an essential role in our understanding of star-formation activity and galaxy evolution. With molecular lines of different species and their different transitions, not only can the chemical composition of the interstellar medium be investigated, but other important physical parameters, such as temperature, pressure, density, and non-collisional pumping mechanisms can be derived as well (e.g., Henkel et al. 1991; Evans 1999; Fukui & Kawamura 2010; Meier & Turner 2012; Meier et al. 2014). New facilities providing wide band and highly sensitive instruments are making weak line surveys and multi-species analyses feasible, and the detections and measurements of a variety of species are helping us to reveal the gas components of galaxies, and how their abundances, densities, and ratios reflect their radiative properties. Multi-species, multi-transition molecular lines can be combined to identify the evolution stage of galaxies (Baan et al. 2014), because different species are sensitive to different physical environments, such as photo dissociation regions (PDRs) dominated by young massive stars, X-rays dominated regions (XDRs) induced by active galactic nuclei (AGNs), and shock waves by cloud-cloud collisions (Aladro et al. 2011; Greve et al. 2009; Costagliola et al. 2011; Viti et al. 2014).

One of the interstellar species that benefits from the upgraded facilities is cyanoacetylene (HC_3N). HC_3N was first detected in 1971 at 9.0977 GHz ($J = 2-1$) in the Galactic star-forming region Sgr B2 (Turner 1971). The critical density of HC_3N is comparable to the widely-used dense gas tracer HCN and can also trace dense molecular gas around star-forming sites. HC_3N has been detected in many star formation regions in the Milky Way with several transitions from centimeter to sub-millimeter (e.g., Suzuki et al. 1992). Due to the small rotational constant (~1/13 of CO), there are many closely spaced rotational transitions of HC_3N (separated by only 9.1 GHz) at centimeter and millimeter wavelengths, and its levels are very sensitive to changes in excitation (Meier & Turner 2012). This makes it easier to conduct multi-transition observations of HC_3N lines than of other dense molecular gas tracers, and can help better understand the excitation conditions of star-forming regions. In contrast, the high-J lines of other dense molecular gas tracers such as HCN and HCO^+ are at very high frequencies, and it is therefore difficult to observe them with ground-based telescopes. Another advantage of using HC_3N lines is that HC_3N is very likely optically thin even in low-J transitions, due to the relatively low abundance (Irvine et al. 1987; Lindberg et al. 2011); low opacity is important for accurate estimate of dense molecular gas mass for the study of the relationship between dense molecular gas and star formation (Gao & Solomon 2004a,b; Wang et al. 2011; Zhang et al. 2014).

There have been efforts to detect HC_3N in nearby galaxies, mainly in millimeter band. Observations suggest that HC_3N is related to the warm, dense, star-forming gas, and is easily dissociated by UV radiation (Henkel et al. 1988; Costagliola et al. 2011; Lindberg et al. 2011; Aladro et al. 2011, 2015). HC_3N was found to be unusually luminous in NGC 4418, and it

Table 1. The source list of the 21 galaxies observed for HC_3N emission using the Effelsberg 100m and the SMT telescope.

Galaxy	RA (J2000) Dec		V_{Helio}	Distance	log L_{IR}	ΔV_{CO}	Telescope
	h m s	° ′ ″	(km s^{-1})	(Mpc)	($L_\odot$)	(km s^{-1})	
(1)	(2)	(3)	(4)	(5)	(6)	(7)	(8)
NGC 520	01 24 34.9	+03 47 30.0	2281	30.22	10.91	270	Effelsberg
NGC 660	01 43 02.4	+13 38 42.0	850	12.33	10.49	280	Effelsberg
NGC 891	02 22 33.4	+42 20 57.0	528	8.57	10.27	110	Effelsberg
NGC 972	02 34 13.4	+29 18 41.0	1543	20.65	10.67	220	Effelsberg
NGC 1068	02 42 41.4	−00 00 45.0	1137	13.7	11.27	280	Effelsberg & SMT
IC 342	03 46 48.5	+68 05 46.0	31	4.60	10.17	72.8[a]	Effelsberg & SMT
UGC 2855	03 48 20.7	+70 07 58.0	1200	19.46	10.75	...	Effelsberg
UGC 2866	03 50 14.9	+70 05 40.9	1232	20.06	10.68	...	Effelsberg
NGC 1569	04 30 49.0	+64 50 53.0	−104	4.60	9.49	90	Effelsberg
NGC 2146	06 18 39.8	+78 21 25.0	882	16.47	11.07	320	Effelsberg & SMT
NGC 2403	07 36 51.3	+65 36 29.9	161	3.22	9.19	90	Effelsberg
M 82	09 55 53.1	+69 40 41.0	187	3.63	10.77	150	Effelsberg & SMT
NGC 3079	10 01 57.8	+55 40 47.0	1116	18.19	10.73	380	Effelsberg
NGC 3310	10 38 45.9	+53 30 12.0	993	19.81	10.61	140	Effelsberg
M 66	11 20 15.0	+12 59 30.0	727	10.04	10.38	180	Effelsberg
IC 694	11 28 33.8	+58 33 45.0	3120	47.74	11.63	250	Effelsberg[b] & SMT
NGC 3690	11 28 30.8	+58 33 43.0	3120	47.74	11.32	260	Effelsberg[b] & SMT
Mrk 231	12 56 14.2	+56 52 25.0	12600	171.84	12.51	167	Effelsberg
Arp 220	15 34 57.1	+23 30 10.0	5352	79.90	12.21	360	Effelsberg & SMT
NGC 6240	16 52 58.9	+02 24 03.0	7160	103.86	11.85	420	SMT
NGC 6946	20 34 52.6	+60 09 12.0	53	5.32	10.16	130	Effelsberg & SMT

Notes. The columns are: (1) galaxy name; (2) and (3) coordinates; (4) heliocentric velocities; (5) distances; (6) total infrared luminosities (from Sanders et al. 2003); (7) CO 1−0 line width (FWHM) of the galaxies; and (8) the telescope these galaxies were observed with. [(a)] For IC 342, the ΔV is of CO 2−1 from Gao & Solomon (2004a); for other galaxies ΔV are of CO 1−0 from Young et al. (1995). [(b)] The Arp 299 system (IC 694 and NGC 3690) was observed as a single pointing by the Effelsberg.

is attributed to its high abundance (10^{-7}) as well as the intense radiation field in the dense and warm gas at the center of NGC 4418 (Aalto et al. 2007; Costagliola & Aalto 2010). Meier & Turner (2005, 2012), Meier et al. (2011, 2014) presented high-resolution observations of HC_3N (J = 5−4, 10−9, 12−11 and 16−15) of a few very nearby galaxies, and gave detailed analysis of the galactic structures and morphology traced by HC_3N and other dense gas tracers (HNC, HCN, CS, etc.). However, these results are still limited by their sample size, and the chemical process of HC_3N (both formation and destruction) is still unclear. Larger samples are still necessary for analyzing the properties of HC_3N and how it relates to other galactic parameters. In this paper, we present the first systematic survey of HC_3N (J = 2−1) and HC_3N (J = 24−23) in a relatively large sample of nearby galaxies, and the results are compared with the observations of HC_3N in other transitions. The critical densities of HC_3N J = 2−1 and HC_3N J = 24−23 are approximately 3×10^3 cm^{-3} and 4×10^6 cm^{-3}, respectively, and the upper state energies (E_u) of the two transitions are 1.3 K and 131 K, respectively (Costagliola & Aalto 2010).

2. Observations and data reduction

We selected nearby infrared bright galaxies (Sanders et al. 2003) with IRAS 60 μm flux greater than 30 Jy and declination greater than −21° to carry out this survey. It is not a complete sample, but is representative of infrared bright galaxies. The sample consists of 21 galaxies. We note that, due to the different beam size of the two telescopes we used, the merger Arp 299 (IC 694 and NGC 3690) was observed as a single pointing by Effelsberg 100-m, while the two galaxies were observed separately by the SMT 10-m.

2.1. HC_3N 2−1 observations with the Effelsberg 100-m

HC_3N (J = 2−1) (ν_{rest} = 18.196 GHz) of 20 galaxies was observed with the Effelsberg 100-m telescope in 2010. The half power beam width (HPBW) is 46.5″ at 18 GHz for the 100-m telescope. We used the 1.9 cm band receiver (500 MHz bandwidth with 16384 channels correlator setup) that provided ∼8300 km s^{-1} velocity coverage and ∼0.5 km s^{-1} velocity resolution during the observations. Position-switching mode with beam-throws of approximately ±2′ was used. Pointing and focus were checked approximately every two hours. The typical system temperature of the Effelsberg observations was approximately 46 K. The on-source time for each galaxy is approximately 14−47 min. The weather during the observations is not ideal, and the baselines of many sources are affected and induced artificial features that are difficult to remove.

2.2. HC_3N 24−23 observations with the SMT 10-m

HC_3N (J = 24−23) (ν_{rest} = 218.324 GHz) of nine galaxies was observed in 2009 with the SMT 10-m telescope. The HPBW is approximately 33″ at ∼218 GHz for SMT, and a single pointing was used for each galaxy toward their central positions. We used the ALMA Sideband Separating Receiver and the Acousto-Optical-Spectrometers (AOS), which have dual polarization, 970 MHz (∼1300 km s^{-1}) bandwidth and 934 kHz channel spacing. Observations were carried out with the beam-switching

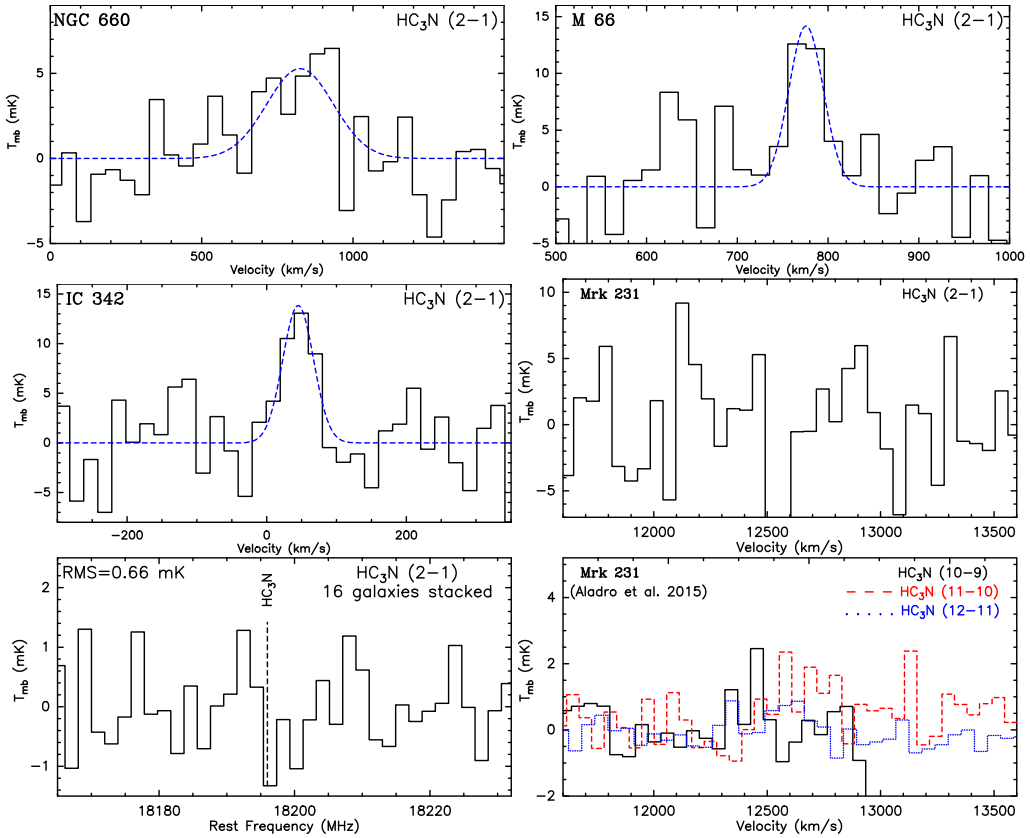

Fig. 1. Spectra of the detected $HC_3N(J = 2-1)$ in NGC 660, M 66, and IC 342 by the Effelsberg. The bottom row also shows the stacked spectra and the spectra of Mrk 231 from Aladro et al. (2015). Blue dashed lines are the Gaussian fit of the HC_3N 2-1 lines. The temperature scale is T_{mb} in mK.

mode with a chop throw of 2′ in azimuth (AZ) and a chopping frequency of 2.2 Hz. Pointing and focus were checked approximately every two hours by measuring nearby QSOs with strong millimeter continuum emission. The typical system temperature at 218 GHz was less than 300 K, and the on-source time for each galaxy was ∼60−168 min.

2.3. Data reduction

The basic parameters of our sample galaxies are listed in Table1. The data were reduced with the CLASS program of the GILDAS[1] package. First, we checked each spectrum and discarded the spectra with unstable baselines. Most of the Effelsberg spectra do not have flat baselines, but over several hundred km s^{-1} near the line, the baselines can still be fixed. In the SMT spectra, the image signal of strong CO 2−1 in the upper sideband affects the baseline of the lower sideband and for M 82 and Arp 220, the HC_3N 24−23 is contaminated. However, for other galaxies, the image CO line does not affect the HC_3N line. Then, we combined spectra with both polarizations of the same source into one spectrum. Depending on the quality of the spectral baselines, a first-order or second-order fitting was used to subtract baselines from all averaged spectra. The identifications of the transition frequencies of HC_3N have made use of the NIST database Recommended Rest Frequencies for Observed Interstellar Molecular Microwave Transitions[2].

To reduce the noise level, the spectra were smoothed to velocity resolutions ∼20−40 km s^{-1}. The velocity-integrated intensities of the HC_3N line were derived from the Gaussian fit of the spectra, or integrated over a defined window if the line profiles significantly deviated from a Gaussian. The intensities were calculated using $I = \int T_{mb} dv$, where T_{mb} is the main beam brightness temperature. Molecular line intensity in antenna temperature (T_A^*) was converted to main beam temperature T_{mb} via $T_{mb} = T_A^*/MBE$, with the main beam efficiency MBE = 53% at 18 GHz for Effelsberg telescope, and 70% at 218 GHz for SMT during the observations. The flux density was then derived from T_{mb}, using $S/T_{mb} = 0.59$ Jy/K for the Effelsberg telescope, and 24.6 Jy/K for the SMT.

3. Results and discussion

The spectral measurements and estimated intensities of the HC_3N lines, including RMS noise and on-source time, are listed in Table 2 (HC_3N 2−1) and Table 3 (HC_3N 24−23).

3.1. HC_3N 2−1

Among the 20 galaxies observed by Effelsberg 100-m telescope, HC_3N 2−1 is detected in three galaxies: IC 342, NGC 660, and M 66 (See Fig. 1). This is the first report of HC_3N 2−1 detection in external galaxies, although limited by the signal to noise ratio (SNR), the detection rate is low.

IC 342: IC 342 has the strongest peak intensity ($T_{mb} \sim 14$ mK) of HC_3N 2−1 in the sample, which is approximately twice the strength of the $HC_3N(9-8)$ line of IC 342 detected by the IRAM 30-m telescope (Aladro et al. 2011), while the line width

[1] http://iram.fr/IRAMFR/GILDAS/
[2] http://www.nist.gov/pml/data/micro/index.cfm

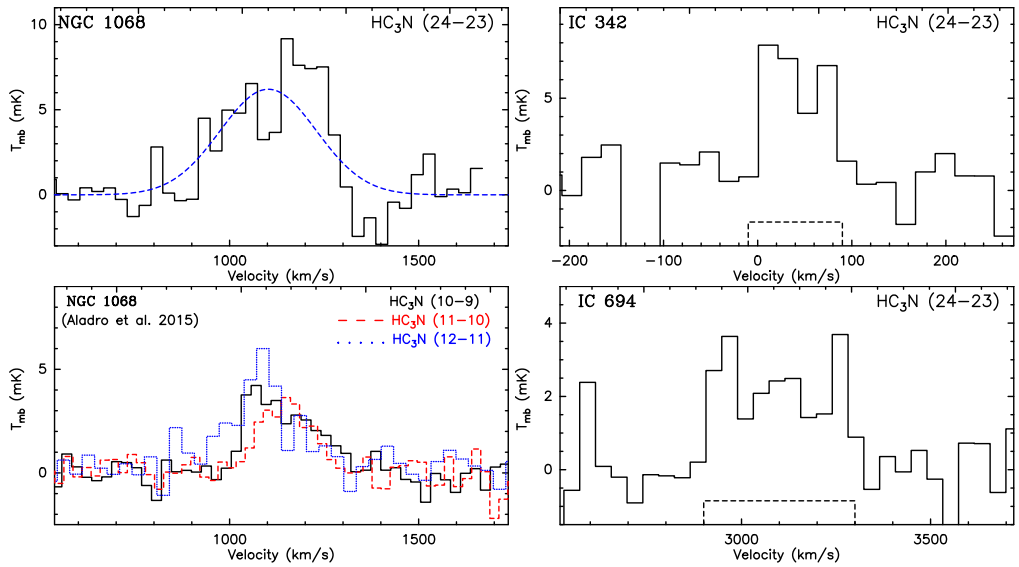

Fig. 2. Spectra of detected $HC_3N(J = 24-23)$ in NGC 1068, IC 342 and IC 694 by the SMT. At the *bottom left*, the spectra of NGC 1068 from Aladro et al. (2015) are shown for comparison. Blue dashed line is the Gaussian fit. We note that, in IC 694, it is difficult to distinguish the HC_3N emission from the possibly blended H_2CO lines. The temperature scale is T_{mb} in mK.

(full width at half medium (*FWHM*) $\sim$ 60 km s^{-1}) is similar to their result.

NGC 660: the detected HC_3N 2−1 in NGC 660 has a similar line width (*FWHM* $\sim$ 294.7 km s^{-1}) to CO 1−0 ($\sim$280 km s^{-1}). While the HC_3N survey by Lindberg et al. (2011) did not observe NGC 660, its 10−9 and 12−11 transitions were not detected by Costagliola et al. (2011). This difference in the detection of HC_3N lines may imply that there is little warm and dense gas content in NGC 660, thus the high-J HC_3N lines can not be excited.

M 66: in M 66, HC_3N 2−1 is only detected on the approximately 2σ level, but this is the first tentative detection of HC_3N in M 66. It was not observed by Costagliola et al. (2011) or Lindberg et al. (2011).

Non-detections: due to the poor quality (and probably insufficient integration time) of the HC_3N 2−1 data, 16 out of 19 galaxies were not detected. Assuming their line width is approximate to CO 1−0 line width (FWHM, from Young et al. 1995), we derive upper limits of the integrated intensity for each galaxy (2σ, where σ = RMS $\sqrt{\delta V \cdot \Delta V}$) and show them in Table 2. Note that the line width of HC_3N is likely narrower than that of CO, and such an assumption might overestimate the upper limits of integrated intensity and is therefore only an approximate estimate. The upper limits are in the range of $\sim$0.3−1.2 K km s^{-1}. For those non-detection galaxies, we also stack their spectra together, weighted by the RMS level of each galaxy, to examine whether or not a cumulated signal can be obtained (see Fig. 1). Although the RMS of the the stacking HC_3N 2−1 spectrum is reduced down to 0.66 mK, we do not see any signs of emission (at a resolution of 30 km s^{-1}). Since these galaxies have similar line widths (100−400 km s^{-1}), we can estimate the stacked upper limit assuming a line width of 200 km s^{-1} based on the RMS (0.66 mK) of the stacked spectra. Thus, the 2σ upper limit of these galaxies is approximately 0.26 K km s^{-1}. To eliminate the possible effect induced by different line widths of galaxies, we also tried to group the non-detection galaxies based on their CO line width. Galaxies with CO FWHM (Table 1) wider than 200 km s^{-1} are stacked as one group, and other galaxies are stacked as another group. Neither group shows any signs of emission.

3.2. HC_3N 24−23

Among the nine galaxies observed by SMT, $HC_3N(J = 24-23)$ is detected in three galaxies: IC 342, NGC 1068 and IC 694 (Fig. 2).

IC 342: HC_3N 24−23 of IC 342 was previously detected and measured by Aladro et al. (2011), and our observation obtains consistent results, although by comparison to their observation, we do not detect H_2CO simultaneously. In our observations, IC 342 is the only galaxy detected in both 2−1 and 24−23 transitions. The line center and width of the two transitions are similar, considering observational uncertainties. This might imply that the two transitions have similar emitting areas. Furthermore, the ratio between the integrated intensities of HC_3N 24−23 and HC_3N 2−1 is approximately 0.6.

NGC 1068: in NGC 1068, the integrated intensity of HC_3N 24−23 is approximately 2.0 K km s^{-1} (in T_{mb}), which is stronger than that of HC_3N 10−9 ($\sim$1.1 K km s^{-1}) reported by Costagliola et al. (2011). This may imply that there is sufficient warm and dense gas, which is able to excite the high transition HC_3N 24−23 line. Besides, it could also be affected by the strong AGN signature of this galaxy (Wang et al. 2014; Tsai et al. 2012).

IC 694: previous observations only obtained upper limits of HC_3N 12−11 for IC 694 (Lindberg et al. 2011). In our observations, a tentative detection in IC 694 ($>2\sigma$) is obtained. The line profile of IC 694 obviously deviates from a Gaussian, so we derive the HC_3N intensity by integrating the line within a window of 400 km s^{-1} width (Table 3).

Table 2. HC_3N 2-1 spectral measurements.

Source	On-time	RMS	δV	ΔV	V_0	$I(HC_3N)$	$S(HC_3N)$	$\frac{HC_3N\ 2-1}{HCN\ 1-0}$
	(min)	(mK)	(km s^{-1})	(km s^{-1})	(km s^{-1})	(K km s^{-1})	(Jy km s^{-1})	
(1)	(2)	(3)	(4)	(5)	(6)	(7)	(8)	(9)
NGC 660	28	4.2	32.2	260.7 (90.6)	825 (36)	1.47 (0.40)	0.86 (0.24)	~0.034[a]
IC 342	20	6.5	20.1	52.0 (12.9)	45 (6)	0.77 (0.18)	0.45 (0.11)	~0.005[b]
M 66	18	7.0	20.1	44.8 (17.7)	775 (7)	0.68 (0.21)	0.4 (0.12)	~0.114[c]
NGC 520	14	5.7	...	...	...	<1.02	<0.6	<0.087[d]
NGC 891	30	2.3	...	...	...	<0.26	<0.15	<0.033[e]
NGC 972	33	3.8	...	...	...	<0.61	<0.36	...
NGC 1068	25	4.0	...	...	...	<0.73	<0.43	<0.013[f]
UGC 2855	23	4.9	...	...	...	<0.76*	<0.45	...
UGC 2866	22	3.6	...	...	...	<0.56*	<0.33	...
NGC 1569	33	3.0	...	...	...	<0.31	<0.18	...
NGC 2146	24	3.4	...	...	...	<0.67	<0.39	<0.021[e]
NGC 2403	30	3.2	...	...	...	<0.33	<0.19	...
M 82	26	5.5	...	...	...	<0.73	<0.43	<0.011[e]
NGC 3079	19	5.5	...	...	...	<1.17	<0.69	<0.225[e]
NGC 3310	36	2.3	...	...	...	<0.29	<0.17	...
IC 694+NGC3690	47	4.2	...	...	...	<0.72	<0.42	<0.158[g]
Mrk 231	44	6.4	...	...	...	<0.91	<0.54	<0.191[g]
Arp 220	26	4.5	...	...	...	<0.94	<0.55	<0.069[h]
NGC 6946	28	5.1	...	...	...	<0.64	<0.38	<0.018[e]

Notes. All the temperature scales are T_{mb}. The columns are: (1) galaxy name; (2) on-source time for each galaxy; (3) RMS noise of the smoothed spectrum; (4) velocity resolution of the smoothed spectrum; (5) line width (FWHM) of the Gaussian fit of the line (if available); (6) HC_3N emission line center; (7) integrated intensity (and errors) of HC_3N 2−1 emission. For those non-detections, 2σ upper limits are presented (see text in Sect. 3.1); (8) integrated flux density, and (9) flux density ratio between HC_3N 2−1 and HCN 1−0. [(*)] The upper limits of the two galaxies are derived assuming a 200 km s^{-1} line width. HCN 1−0 data from: [(a)] Baan et al. (2008); [(b)] Nguyen et al. (1992); [(c)] Krips et al. (2008); [(d)] Solomon et al. (1992); [(e)] Gao & Solomon (2004a); [(f)] Aladro et al. (2015); [(g)] Jiang et al. (2011); [(h)] Wang et al. (2016).

Table 3. HC_3N 24−23 spectral measurements.

Source	On-time	RMS	δV	ΔV	V_0	$I(HC_3N)$	$S(HC_3N)$	$\frac{HC_3N\ 24-23}{HCN\ 1-0}$
	(min)	(mK)	(km s^{-1})	(km s^{-1})	(km s^{-1})	(K km s^{-1})	(Jy km s^{-1})	
(1)	(2)	(3)	(4)	(5)	(6)	(7)	(8)	(9)
NGC 1068	121	1.2	39.1	257.3 (24.0)[a]	1102 (13)	2.03 (0.18)	49.9 (4.4)	~0.59
IC 342	132	2.7	20.9	100[b]	43	0.47 (0.12)	11.6 (3.0)	~0.12
IC 694	127	0.87	41.7	400[b]	3095	0.90 (0.11)	22.1 (2.7)	~2.76
NGC 2146	115	1.01	20.9	320[c]	...	<0.17	4.2	<0.26
M 82	60	3.0	20.9	150[c]	...	<0.34	8.4	<0.26
NGC 3690	139	0.73	42.0	260[c]	...	<0.15	3.7	<1.27
ARP 220	162	0.75	39.1	420[c]	...	<0.19	4.7	<0.48
NGC 6240	97	0.92	20.1	420[c]	...	<0.17	4.2	<1.15
NGC 6946	168	1.76	21.0	130[c]	...	<0.18	4.4	<0.26

Notes. Columns are the same as Table 2. [(a)] FWHM from the Gaussian fitting and error. [(b)] Line window (full width) used to derived the integrated intensity. [(c)] CO width from Young et al. (1995) that are used to derived the upper limits.

We note that, in NGC 1068 and IC 694, HC_3N 24−23 is possibly blended with H_2CO 3(0, 3)−2(0, 2) emission (f_ν = 218.22219 GHz). The upper state energy of this para-H_2CO line is approximately 10.5 K, which is likely to be excited in these cases. The H_2CO line is shifted by 141.1 km s^{-1} or −102 MHz from the HC_3N 24−23 line, and it is unclear how much intensity of HC_3N 24−23 in NGC 1068 and IC 694 is contributed by H_2CO (see Fig. 2). We still lack sufficient data to disentangle this issue, and can only compare with other observations. For example, in the observation of M 82 by Ginard et al. (2015), they showed that near the frequency of 145 GHz, H_2CO 2(0, 1)−1(0, 1) is as strong as HC_3N 16−15. H_2CO is not detected in M 82 in the 3 mm band (Aladro et al. 2015). In the observations toward NGC 4418 by Aalto et al. (2007), they showed that HC_3N 16−15 is blended with H_2CO, and H_2CO may contribute 20% of the total integrated line intensity.

Non-detections: the spectra of M 82 and Arp 220 are seriously contaminated by the image signal of CO 2−1 from the upper side-band (ν = 230 GHz), which is strong and wide and therefore difficult to remove. As a consequence, we could not extract the spectrum of HC_3N properly. We treat the HC_3N 24−23 in M 82 and Arp 220 as non-detections, and their 2σ upper

limits are also only indicative. Although not contaminated by adjacent CO image signal, HC_3N 24−23 was not detected in NGC 2146, NGC 6946, NGC 3690, or NGC 6240. For these non-detections, we present a 2σ upper limit of the integrated intensity of HC_3N 24−23 in Table 3. Only four galaxies are not contaminated by CO image signal, thus no stacking is implemented for their HC_3N 24−23 spectra.

3.3. Discussion: HC_3N in galaxies

The HPBW of SMT and Effelsberg observations are 33″ and 46″, respectively, which should be able to cover the bulk of the sample galaxies, especially the galaxy center. Thus, our observations should be able to cover the region where the majority of dense gas resides. However, with single-dish observations, we cannot constrain the emission size of either HC_3N 2−1 or HC_3N 24−23, and cannot easily estimate the filling factors. Along with the large uncertainty of the emission intensity measurements, it is difficult to estimate the brightness temperature of the sample.

To better understand the excitation environment of HC_3N, the effect of free-free and synchrotron emission near 18 GHz should also be taken into account, as they are more prominent than that in the millimeter band that is dominated by dust thermal emission. We detect HC_3N 2-1 lines in emission and not in absorption, and this may be due to the fact that the beam filling factor of the HC_3N gas is higher than the radio continuum. In the high-resolution radio observations toward a few nearby galaxies (Tsai et al. 2006), it is found that compact radio sources contribute 20−30% of the total 2 cm (15 GHz) emission from the central kiloparsec of these galaxies. In contrast, the distribution of gas with moderate critical density such as HC_3N 2−1 is likely more diffuse.

Comparing to other dense molecular gas tracers such as the popular HCN and HCO^+, HC_3N is generally optically thin in galaxies owing to its relatively low abundance, which makes it an ideal dense gas tracer for calculating the column density and/or mass of molecular hydrogen content of galaxies. In the observations by Lindberg et al. (2011) and Costagliola et al. (2011), a low detection rate of HC_3N was reported and was explained as the intrinsically faint emission of HC_3N, and our stacked result also implies that the HC_3N is relatively weak in the non-detected galaxies (2σ upper limit = 0.14 K km s^{-1}), which is also in favor of this explanation. The non-detection in M 82 is consistent with the low abundance of HC_3N in M 82 suggested by Aladro et al. (2011); HC_3N traces a nascent starburst of galaxy, and can easily be destroyed by the UV radiation in PDRs, which is ubiquitous in active galaxies.

In very recent line surveys of a small number of local active galaxies (AGN and/or starbursts, Aladro et al. 2015; Costagliola et al. 2015), several HC_3N transitions in 3 mm band (HC_3N J = 10−9, J = 11−10 and J = 12−11) were detected. The ALMA observations by Costagliola et al. (2015) even reported the HC_3N J = 32−31 rotational transition, and some of the vibrationally excited HC_3N lines. The latest high-resolution line surveys in a number of very nearby galaxies (Meier & Turner 2005, 2012) and Meier et al. (2014, 2015) show that the derived HC_3N abundances (on ∼100 pc, approximately GMC scales) are approximately several 10^{-10} (relative to H_2), which is approximately an order of magnitude lower than the abundance of HCN and some other molecules.

The results in Aladro et al. (2015) show that, the HC_3N fractional abundance is generally several times lower than that of HCN, HCO^+, and CS, and comparing to other AGN or starburst galaxies in their sample, HC_3N abundance is significantly higher in the two ultra luminous infrared galaxies (ULIRGs) Arp 220 and Mrk 231, implying that it is well-suited for studying the activity of ULIRGs. Besides, there was no obvious evidence of AGN having an effect on the intensity of HC_3N. Four galaxies in our sample (NGC 1068, M 82, Mrk 231 and Arp 220) were also studied in Aladro et al. (2015). We compared our data with their results, and the HC_3N spectra of Mrk 231 and NGC 1068 from Aladro et al. (2015) are shown in Figs. 1 and 2, to be compared with the non-detection of HC_3N 2−1 in Mrk 231, and the detection of HC_3N 24−23 in NGC 1068, respectively. Their results show that, in 3mm band, the intensities between the three transitions of HC_3N (10−9, 11−10 and 12−11) differ very little, and the peak temperature ($T_{\rm mb}$) of HC_3N is ∼4 mK for NGC 1068, ∼11 mK for M 82, ∼1.1−1.7 mK for Mrk 231, and ∼10 mK for Arp 220. In our results, the detection of HC_3N 24−23 in NGC 1068 shows a peak $T_{\rm mb}$ ∼ 7 mK, while the non-detections of HC_3N 2−1 in Mrk 231 and Arp 220 show that, the RMS we have (∼4−6 mK) might not be low enough to detect the HC_3N lines. Here, we conclude that, besides the low abundance of HC_3N, insufficient integration time and non-ideal observing conditions are the main causes of the low detection rate of HC_3N.

It would be interesting to compare the intensity ratios between HC_3N and other dense gas tracers, such as HCN and HCO^+. In the HC_3N survey by Lindberg et al. (2011), ratios such as HC_3N/HCN were used to compare HC_3N between galaxies. Based on that ratio, IC 342 and M 82 were classified as HC_3N-luminous galaxies. In our observation, we detect both HC_3N 2−1 and HC_3N 24-23 in IC 342, but neither HC_3N transition is detected in M 82. On the other hand, we obtained HC_3N 24−23 detections in NGC 1068, which was classified as a HC_3N-poor galaxy in Lindberg et al. (2011). In the sample of some nearby galaxies observed by Aladro et al. (2015), the ratio between the peak temperature ($T_{\rm mb}$) of HC_3N/HCN or HC_3N/HCO^+also showed large variation. In NGC 253 and M 82, HC_3N 10−9 is only ∼1/20 the strength of HCO^+ 1−0, while in Arp 220, HC_3N 10−9 is nearly as strong as HCO^+ 1−0. In our results, such line ratios also show large diversity. It is not yet clear how to interpret the ratio between HC_3N and other molecular lines, and more data of HC_3N in different transitions would be helpful to disentangle its properties in different types of galaxies.

Our observations and other works have presented detection of HC_3N emission lines from nearly 18 GHz up to ∼292 GHz. The newly commissioned Tianma 65 m telescope in Shanghai, China, is able to observe low transition HC_3N emission, and has great potential for further HC_3N 2−1 surveys for large samples of galaxies.

4. Summary

We carried out single-dish observations toward a sample of nearby gas-rich galaxies with the Effelsberg telescope and the Submillimeter Telescope. These are the first measurements of HC_3N 2-1 in a relatively large sample of external galaxies.

HC_3N(J = 2−1) (ν = 18.196 GHz) was observed with the 100-m telescope in 20 galaxies and only three galaxies are detected (>3σ): IC 342, M 66 and NGC 660. These are the first measurements of HC_3N 2−1 reported in external galaxies, and the first HC_3N detections in M 66. We stack the spectra of those non-detections, yet there is still no sign of HC_3N emission. The 2σ upper limit of HC_3N intensity from the stacked spectrum is approximately 0.12 K km s^{-1}.

$HC_3N(J = 24-23)$ ($\nu = 218.324$ GHz) was observed in nine galaxies with the SMT, and was detected in three galaxies: IC 342, IC 694, and NGC 1068.

IC 342 is the only galaxy detected in both HC_3N 2−1 and HC_3N 24−23 transitions in our observations, and the two transitions have similar line centers and widths, suggesting a similar emitting area. The ratio of integrated intensity of HC_3N 24−23/HC_3N 2−1 is approximately 0.82. Due to the contamination of CO 2−1 image signal in the upper sideband, M 82 and Arp 220 are treated as non-detections of HC_3N 24−23.

The ratios between HC_3N and HCN, HCO^+ show large variation among the galaxies with HC_3N detections, implying different behavior of the molecular lines in galaxies. More samples are needed to better understand the relationship between HC_3N and other molecules.

Acknowledgements. Based on observations with the 100-m telescope of the MPIfR (Max-Planck-Institut für Radioastronomie) at Effelsberg, and the Submillimeter Telescope (SMT). The SMT is operated by the Arizona Radio Observatory (ARO), Steward Observatory, University of Arizona. We thank the staff of the Effelsberg telescope and the SMT for their kind help and support during our observations. This project is funded by China Postdoctoral Science Foundation (grant 2015M580438), National Natural Science Foundation of China (grant 11420101002, 11311130491, 11590783 and 11603075), and the CAS Key Research Program of Frontier Sciences. This research has made use of NASA's Astrophysics Data System, and the NASA/IPAC Extragalactic Database (NED), which is operated by the Jet Propulsion Laboratory, California Institute of Technology, under contract with the National Aeronautics and Space Administration.

References

Aalto, S., Monje, R., & Martín, S. 2007, A&A, 475, 479
Aladro, R., Martín-Pintado, J., Martín, S., Mauersberger, R., & Bayet, E. 2011, A&A, 525, A89
Aladro, R., Martín, S., Riquelme, D., et al. 2015, A&A, 579, A101
Baan, W. A., Henkel, C., Loenen, A. F., Baudry, A., & Wiklind, T. 2008, A&A, 477, 747
Baan, W. A., Loenen, A. F., & Spaans, M. 2014, MNRAS, 445, 3331
Costagliola, F., & Aalto, S. 2010, A&A, 515, A71
Costagliola, F., Aalto, S., Rodriguez, M. I., et al. 2011, A&A, 528, A30
Costagliola, F., Sakamoto, K., Muller, S., et al. 2015, A&A, 582, A91
Evans, II, N. J. 1999, ARA&A, 37, 311
Fukui, Y., & Kawamura, A. 2010, ARA&A, 48, 547
Gao, Y., & Solomon, P. M. 2004a, ApJS, 152, 63
Gao, Y., & Solomon, P. M. 2004b, ApJ, 606, 271
Ginard, D., Fuente, A., García-Burillo, S., et al. 2015, A&A, 578, A49
Greve, T. R., Papadopoulos, P. P., Gao, Y., & Radford, S. J. E. 2009, ApJ, 692, 1432
Henkel, C., Schilke, P., & Mauersberger, R. 1988, A&A, 201, L23
Henkel, C., Baan, W. A., & Mauersberger, R. 1991, A&A, 3, 47
Irvine, W. M., Goldsmith, P. F., & Hjalmarson, A. 1987, in Interstellar Processes, eds. D. J. Hollenbach & H. A. Thronson, Jr., Astrophys. Space Sci. Lib., 134, 561
Jiang, X., Wang, J., & Gu, Q. 2011, MNRAS, 418, 1753
Krips, M., Neri, R., García-Burillo, S., et al. 2008, ApJ, 677, 262
Lindberg, J. E., Aalto, S., Costagliola, F., et al. 2011, A&A, 527, 17
Meier, D. S., & Turner, J. L. 2005, ApJ, 618, 259
Meier, D. S., & Turner, J. L. 2012, ApJ, 755, 104
Meier, D. S., Turner, J. L., & Schinnerer, E. 2011, AJ, 142, 32
Meier, D. S., Turner, J. L., & Beck, S. C. 2014, ApJ, 795, 107
Meier, D. S., Walter, F., Bolatto, A. D., et al. 2015, ApJ, 801, 63
Nguyen, Q.-R., Jackson, J. M., Henkel, C., Truong, B., & Mauersberger, R. 1992, ApJ, 399, 521
Sanders, D. B., Mazzarella, J. M., Kim, D.-C., Surace, J. A., & Soifer, B. T. 2003, AJ, 126, 1607
Solomon, P. M., Downes, D., & Radford, S. J. E. 1992, ApJ, 387, L55
Suzuki, H., Yamamoto, S., Ohishi, M., et al. 1992, ApJ, 392, 551
Tsai, C.-W., Turner, J. L., Beck, S. C., et al. 2006, AJ, 132, 2383
Tsai, M., Hwang, C.-Y., Matsushita, S., Baker, A. J., & Espada, D. 2012, ApJ, 746, 129
Turner, B. E. 1971, ApJ, 163, L35
Viti, S., García-Burillo, S., Fuente, A., et al. 2014, A&A, 570, A28
Wang, J., Zhang, Z., & Shi, Y. 2011, MNRAS, 416, L21
Wang, J., Zhang, Z.-Y., Qiu, J., et al. 2014, ApJ, 796, 57
Wang, J., Zhang, Z.-Y., Zhang, J., Shi, Y., & Fang, M. 2016, MNRAS, 455, 3986
Young, J. S., Xie, S., Tacconi, L., et al. 1995, ApJS, 98, 219
Zhang, Z.-Y., Gao, Y., Henkel, C., et al. 2014, ApJ, 784, L31